ACS Catalysis

RESEARCH ARTICLE

pubs.acs.org/acscatalysis

Catalytic Roles of Co^0 and Co^{2+} during Steam Reforming of Ethanol on Co/MgO Catalysts

Ayman M. Karim,[†] Yu Su,[†] Mark H. Engelhard,[‡] David L. King,[†] and Yong Wang*[,†,§]

[†]Institute for Interfacial Catalysis and [‡]Environmental Molecular Science Laboratory, Pacific Northwest National Laboratory, Richland, Washington 99354, United States

[§]The Gene and Linda Voiland School of Chemical Engineering and Bioengineering, Washington State University, Pullman, Washington 99164-2710, United States

ABSTRACT: The catalytic roles of Co^0 and Co^{2+} during steam reforming of ethanol were investigated over Co/MgO catalysts. Catalysts with different $Co^0/(Co^0+Co^{2+})$ fraction were prepared through calcination and/or reduction at different temperatures, and the Co^0 fraction was quantified by temperature programmed reduction (TPR) and in situ X-ray photoelectron spectroscopy (XPS). Higher temperature calcination of Co/MgO allowed us to prepare catalysts with more nonreducible Co^{2+} incorporated in the MgO lattice, while lower calcination temperatures allowed for the preparation of catalysts with higher $Co^0/(Co^0+Co^{2+})$ fractions. The catalytic tests on Co^0, nonreducible Co^{2+}, and reducible Co^{2+} indicated that Co^0 is much more active than either reducible or nonreducible Co^{2+} for C−C cleavage and water gas shift reaction. In addition, catalysts with a higher Co^0 surface fraction exhibited a lower selectivity to CH_4.

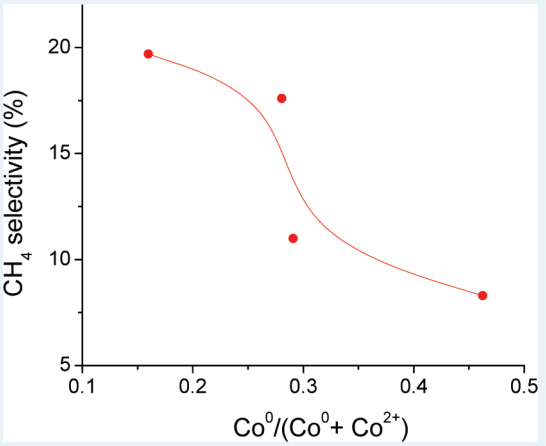

KEYWORDS: ethanol steam reforming, reaction pathway, Co^0, Co^{2+}, XPS, cobalt oxidation state

1. INTRODUCTION

Hydrogen is a clean energy carrier and has been considered for use in fuel cells for pollution-free generation of electricity. H_2 production from ethanol steam reforming (ESR) has recently caught particular attention because of the high H_2 yield and the established technology of ethanol production from biomass.[1,2] Noble metal based catalysts, that is, Rh, Pt, Pd, and Ru, have been extensively investigated[3−8] and have been shown to be highly active for ESR. However, their application is to a large extent limited by their high cost. Transition metal catalysts, such as Ni and Cu, have also been studied,[9−16] but their performance suffers from either low activity and/or fast carbon deposition. Co-based catalysts, in comparison, are less expensive than the noble metals, and have been shown to exhibit high activity and selectivity (to H_2 and CO_2) during ESR.[1,17,18]

The performance of Co-based catalysts is greatly dependent on the catalyst support, preparation method,[19] metal precursor,[17] calcination temperature,[20] and the Co crystalline structure.[21] Several research efforts investigating the reaction mechanism of ESR over Co catalysts have been reported.[1,22−27] Llorca et al. found the reaction pathways are strongly dependent on the support used.[1] With the aid of in situ DRIFTS experiments, they concluded that the first step of ESR over Co/ZnO catalyst was the ethanol dehydrogenation to acetaldehyde.[24] An in situ magnetic study from the same group indicated that both Co^0 and Co^{2+} were observed under the reaction conditions, with an easy exchange between the two species.[22] However, because of the low Co loading and the activity contributed by the support, it was not possible to unambiguously determine whether the active site was Co^0 or Co^{2+}.[22] O' Shea et al. investigated the evolution of Co_3O_4 under *operando* conditions with X-ray diffraction (XRD), and observed that Co_3O_4 was not active, but the evolved material with CoO and Co^0 was active and selective in ESR.[25] On the other hand, Batista et al. believed Co^0 was the only site that was important in ESR.[23] To identify the different roles of Co^0 and Co^{2+}, Tuti et al.[26] investigated bulk Co_3O_4 (both oxidized and reduced), Co supported on MgO and CoO-MgO solid solution. They concluded that the Co^0 was mainly responsible for the reforming of ethanol, while ethanol dehydrogenation could occur on Co^{2+}.[26] However, the specific roles and reactions proceeding on different Co sites have not been identified. In addition, the effect of the different Co^0/Co^{2+} ratios on the activity and product distribution has not been studied.

The goal of this work was to investigate the specific roles of Co^0 and Co^{2+}, as well as the effect of their relative ratio on ESR. MgO was selected as the support because of its ability to form an oxide solid solution with Co, making it possible to stabilize Co^{2+}.[26,28] Catalysts with different Co^0 fraction, $Co^0/(Co^0+Co^{2+})$, were obtained through different calcination and/or reduction pretreatments, and were characterized by N_2 adsorption,

Received: January 11, 2011
Revised: February 2, 2011
Published: February 25, 2011

powder XRD, temperature programmed reduction (TPR), and in situ X-ray photoelectron spectroscopy (XPS). Different reaction pathways on Co^0 and Co^{2+} for ESR were identified, and the effect of steam on Co oxidation state is discussed.

2. EXPERIMENTAL SECTION

2.1. Catalyst Preparation. Two Co/MgO catalysts (10 and 50% Co by weight) were prepared by coprecipitation of magnesium nitrate hexahydrate (98%+, Sigma-Aldrich) and cobalt nitrate hexahydrate (98%+, Sigma-Aldrich) with dropwise ammonium hydroxide until the pH value was about 10.5. The precipitate was then dried at 120 °C for 2 h and calcined at a target temperature (500 or 1000 °C) for 4 h. The Co weight loading in the catalysts was confirmed by inductively coupled plasma mass spectrometry (ICP-MS) analysis to be 9.3% and 52%. MgO was obtained through precipitation of magnesium nitrate hexahydrate (98%+, Sigma-Aldrich) with dropwise ammonium hydroxide until the pH value was about 10.5, then dried at 120 °C for 2 h and calcined at 1000 °C for 4 h. In the following section the catalyst nomenclature of "10Co-MgO-C500-R450" denotes 10 wt % Co on MgO calcined at 500 °C and reduced at 450 °C and "10Co-MgO-NC-R750" denotes 10 wt % Co on MgO without calcination (dried at 120 °C) and reduced at 750 °C.

2.2. XRD Studies. The XRD patterns in θ-2θ scan mode were obtained by a Philips Xpert X-ray diffractometer with a Cu Kα (λ = 0.1543 nm) radiation source between 10° and 80° at a step rate of 1°/min.

2.3. BET and Pore Structures. Multipoint Brunauer−Emmett−Teller (BET) measurements and the pore structure were analyzed by an Autosorb-6 gas sorption system (Quantachrome Corporation), after the samples were degassed overnight at 110 °C.

2.4. TPR Studies. TPR studies were conducted on a Micromeritics (Autochem II) instrument equipped with a thermal conductivity detector (TCD). During each test, about 0.1 g of catalyst was loaded into a U-tube, and was flushed by 5% H_2 in Argon at 30 sccm. The sample was then ramped up from about room temperature to 1000 at 10 °C/min.

2.5. XPS Studies. XPS measurements were performed using a Physical Electronics Quantum 2000 Scanning ESCA Microprobe equipped with a catalytic reactor side chamber and UHV sample transfer system. The catalysts powders were packed into 3.5 mm diameter Mo sample holders and transferred under vacuum <5 × 10^{-9} Torr to the high temperature reactor. H_2 was introduced into the reactor at a flow rate of 100 sccm. The pressure was maintained at 100 Torr using a VAT UHV variable position gate valve and Adaptive Pressure Controller. The catalysts were heated to 450 °C for 1 h. After cooling down to room temperature under H_2 flow, the H_2 was pumped using a series of turbomolecular and sputter ion pumps. The catalyst samples were transferred under vacuum into the photoelectron spectrometer for analysis. This XPS system uses a focused monochromatic Al Kα X-rays (1486.7 eV) source and a spherical section analyzer. The instrument has a 16 element multichannel detector. The X-ray beam used was a 100 W, 100 μm diameter beam that was rastered over a 1.3 mm by 0.2 mm rectangle on the sample. The X-ray beam is incident normal to the sample and the photoelectron detector was at 45° off-normal using an analyzer angular acceptance width of 20° × 20°. High energy resolution spectra were collected using a pass energy of 46.95 eV. The energy scale of the analyzer was calibrated using sputter cleaned Cu and Ag foils. For the $Ag3d_{5/2}$ line, these conditions produced FWHM of better than 0.98 eV. The binding energy (BE) scale is calibrated using the $Cu2p_{3/2}$ feature at 932.62 ± 0.05 eV and Au 4f at 83.96 ± 0.05 eV for known standards. Co/MgO is insulating at room temperature and experienced variable degrees of charging. Low energy electrons at ∼1 eV, 20 μA and low energy Ar^+ ions were used to minimize surface charging. The spectra was shifted in binding energy so that the associated O 1s peak was at 530.0 eV.[29] The main vacuum system pressure was maintained at <5 × 10^{-9} Torr during analysis and pumped using a series of sputter ion pumps.

Using a semiquantitative empirical approach, a spectral curve fitting procedure was applied to determine the sum of photoelectrons for Co^0 and Co^{2+} at the surface of the sample. PHI Multipak (Version 8.2) software was used for peak fitting of the Co2p photoemission spectra. In this approach, a high purity Co metal foil was cleaned in vacuum at <5 × 10^{-9} Torr using 2 kV Ar^+ ion sputtering to obtain a clean Co^0 reference spectra. A photoemission spectrum of the clean cobalt was collected using identical analyzer conditions as the Co/MgO catalyst. The spectral fitting process involved the use of a standard Shirley background subtraction method for removing the spectral background.[30] The asymmetric $Co2p_{3/2}$ main metal peak is measured at 778.2 ± 0.1 eV with a $2p_{3/2}$ to $2p_{1/2}$ splitting of 15.0 eV ± 0.05 eV. The Co^0 $Co2p_{3/2}$ binding energy value compares well to a NIST database average of 778.3 eV ± 0.14 eV and with literature values for Co^0.[31] Fitting of these broad lines combined with a portion of satellite structure has been used for fitting Co^0 spectra.[32,33] In addition to the main lines, two satellite peaks at approximately 2.0 and 4.0 eV higher in binding energy and a very low intensity Co KLL Auger line at 776.5 eV was included to complete the fitting process. For quantification of the relative concentrations of Co^0 and Co^{2+} in the catalysts, we constrained the fitting parameters based on the Co^0 reference. The Co^0 $2p_{3/2}$ and $2p_{1/2}$ peak positions, peak separation, peak area ratio, and FWHM values were locked during the fitting process. The amount of Co^{2+} was calculated from the remaining spectra after fitting the Co^0 components. The Co $2p_{3/2}$ line position for the Co^{2+} was measured at 780.5 eV and is in good agreement with NIST database average values of 780.45 ± 0.17 eV and with literature values.[29]

2.6. Activity Measurements. The catalyst activity measurements were conducted in a stainless steel, single pass, fixed-bed tube reactor (0.5 cm i.d. × 8 cm length). The catalyst, diluted with SiC (5× by weight, particle size was 150−180 μm for the catalyst and SiC), was loaded between two layers of quartz wool inside the reactor. Two K-type thermocouples were placed on the outer wall of the reactor for the measurement of the reactor temperature at the inlet and outlet. The catalyst (30−200 mg) was reduced at 450 °C for 1 h and tested at 450 °C under atmospheric pressure. The reaction temperature of 450 °C was chosen based on our earlier work and other groups' reports on ESR work on Co and Rh based catalysts where 450 °C was found to be an intermediate temperature to get reasonably high activity.[1,18,34] An Acuflow HPLC pump was used to feed the water/ethanol solution (molar ratio of 10:1) and a Brooks mass flow controller (5850E series) was used to control the N_2 flow. The mixture of N_2, water and ethanol was fed to a multichannel vaporizer operating at 160 °C. The ethanol mole fraction in the feed was 0.95%. The effluent of the reactor was analyzed by means of an online HP5890 GC equipped with a flame ionization

Table 1. Textual Properties of the Co-MgO Catalysts

catalyst	surface area (m^2/g)
MgO-C1000	18.4
10Co-MgO-C1000	8.9
50Co-MgO-C1000	4.7
10Co-MgO-C500	12.5

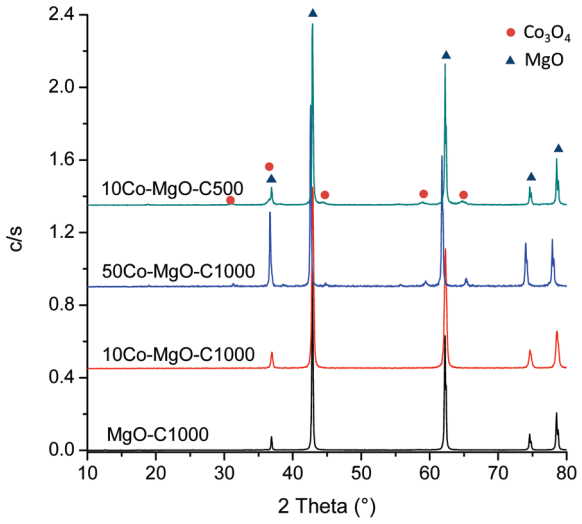

Figure 1. XRD patterns of the calcined Co-MgO catalysts.

detector and a HP plot/Q column to quantify the liquid products and the unreacted ethanol. After condensing the liquid products and unreacted water and ethanol, the gas products were analyzed online by means of a MTI Quad Micro GC (Model Q30L) equipped with MS-5A and PPQ columns and two thermal conductivity detectors. Ethanol conversion is defined by moles of ethanol converted/moles of ethanol fed, whereas the C−C cleavage conversion is calculated by (moles of C_1 products/2)/(moles of ethanol fed). The product selectivity is defined on carbon basis as follows: (moles of product$_i$) × C_i/(moles of ethanol fed × 2), where C_i is the number of carbon atoms in product$_i$. The selectivity to CO_2 (CO or CH_4) in C_1 products is defined as $CO_2/(CO+CO_2+CH_4)$. The gas hourly space velocity was calculated using the measured catalyst bed density of 0.9 g/mL (without dilution). The carbon balance, calculated as carbon in products/carbon fed to the reactor, was at least 90% for all experiments. Deactivation due to coking was observed during the catalytic tests. However, the data reported here were collected during the first 4 h where negligible deactivation was observed. The extent of deactivation was estimated by testing the catalyst after 4 h time on stream at the same conditions as at the beginning of the experiment. Therefore, deactivation and coking can be neglected for the purposes of this study.

3. RESULTS AND DISCUSSION

3.1. BET and Pore Structures. Textural properties of the catalysts are listed in Table 1. MgO exhibited a surface area of 18.4 m^2/g. The surface area for the 10% Co/MgO catalyst did not change significantly following the different pretreatments, and ranged between 9 and 12.5 m^2/g. The surface area for the 50% Co/MgO was significantly lower, 4.7 m^2/g.

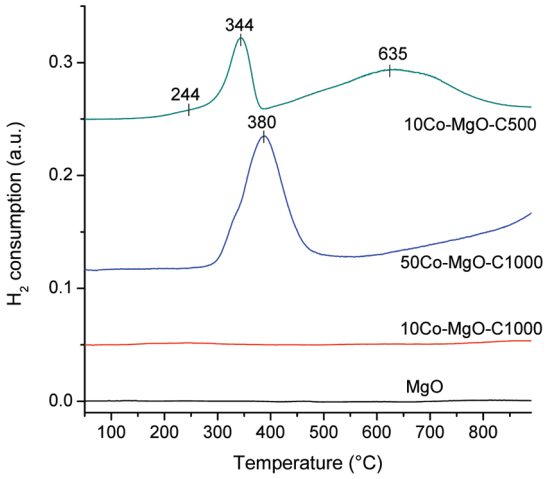

Figure 2. TPR profiles of the Co-MgO catalysts.

3.2. XRD. XRD patterns of the catalysts are shown in Figure 1. Several pronounced peaks at 2θ of about 36.9, 42.9, 62.2, 74.6, 78.5° were observed for all the samples investigated, which can be attributed to MgO. For the 10% Co-MgO catalyst calcined at 500 °C, several peaks corresponding to Co_3O_4 were observed. However, these peaks were not present, and only the MgO crystalline structure was observed after the catalyst was calcined at 1000 °C, suggesting that Co was incorporated into the MgO lattice to form a solid solution. For the 50% Co-MgO-C1000 catalyst, the major diffraction peaks were shifted to a lower 2θ relative to MgO, which can be better seen at the higher 2θ. This can be attributed to the expansion of the lattice when the Co/Mg ratio is increased, which should be expected since Co^{2+} is larger than Mg^{2+}.[28] Small peaks corresponding to Co_3O_4 were also observed; however, the peaks are sharper than for the 10Co-MgO-C500 catalyst, indicating the formation of bigger Co_3O_4 particles with 50Co-MgO-C1000. Co and Mg can form an oxide solid solution over the entire range of compositions because of their similar oxide crystal structure, cation size, and coordination.[28] The formation of Co_3O_4 particles was expected because of a lower calcination temperature for the 50% Co-MgO (1000 °C) compared to the temperatures (>1200 °C) typically used to form the CoO-MgO solid solution.[35]

3.3. TPR. To investigate the reducibility of Co in the Co-MgO catalysts, TPR was conducted, and the corresponding profiles are shown in Figure 2. The TPR profile for MgO is also included as a reference, which shows negligible reduction up to 1000 °C. No pronounced reduction peak was observed on the 10% Co-MgO catalyst calcined at 1000 °C, indicating that most of the Co was incorporated into the lattice structure of MgO, as indicated by the XRD results in Figure 1. In contrast, two main reduction peaks at 344 °C (with a small shoulder at 244 °C) and 635 °C were seen with the 10Co-MgO-C500 catalyst. It has been generally accepted that the reduction of Co_3O_4 proceeds in a two step process, Co_3O_4 to CoO, and CoO to Co,[36,37] and one could expect the TPR profiles to present one peak for each step. However, because of the effects of particle size and strength of interaction with the support on the reduction kinetics, the number of TPR peaks and their location can vary significantly.[38,39] For example, because of a broad particle size distribution, TPR of bulk Co_3O_4 exhibited only one broad reduction peak centered at about 420 °C.[26] For Co supported on silica, a higher temperature was required for the reduction of smaller cobalt

dx.doi.org/10.1021/cs200014j |ACS Catal. 2011, 1, 279–286

Table 2. Fraction of Co^0, $Co^0/(Co^0+Co^{2+})$ for the Co-MgO Catalysts As Estimated from the TPR profiles and XPS Spectra[a]

catalyst	10Co-MgO-C1000-R450	50Co-MgO-C1000-R450	10Co-MgO-C500-R450	10Co-MgO-C500-R750	10Co-MgO-NC-R750
TPR	0.005	0.07	0.2	0.57	NA[b]
XPS	0.16	0.28	0.29	0.46	0.59
Co/Mg atomic ratio[c]	0.42	2.28	0.29	0.33	0.33

[a] Co/Mg atomic ratio from the XPS spectra is also included. [b] TPR not available. [c] By XPS.

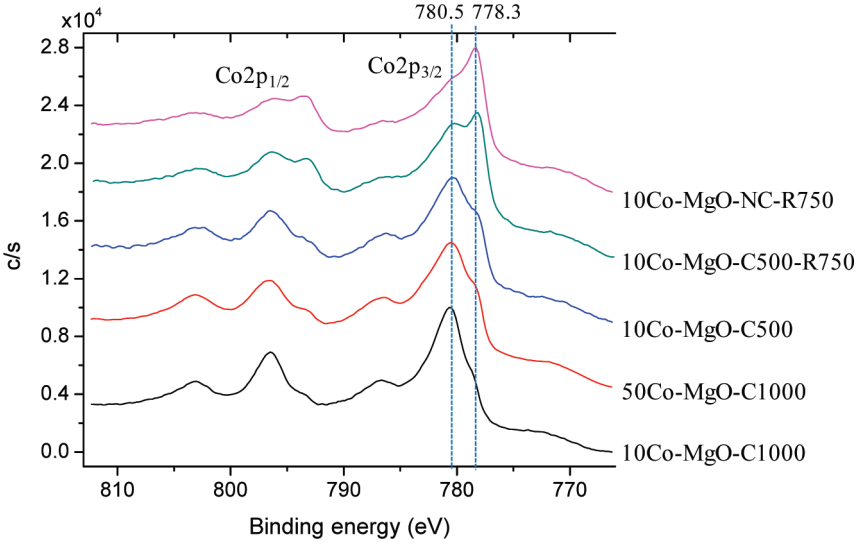

Figure 3. X-ray spectra recorded in the Co 2p region for the Co-MgO catalysts. All catalysts were reduced in situ at 450 °C for 1 h prior to XPS analysis. Peaks at 778.3 and 780.5 eV, respectively, are characteristic of Co^0 and Co^{2+}.

oxide particles compared to the larger particles, which was attributed to the stronger interaction of the smaller particles with the support.[40] As a result, the peak at 344 °C (with a small shoulder at 244 °C) can be ascribed to the two step reduction of Co_3O_4 to Co having a weak interaction with MgO, while the peak at a high reduction temperature of 632 °C can be attributed to the reduction of Co having a strong interaction with MgO. Only one broad peak at 380 °C (in the range of 300 to 500 °C) can be seen over the 50Co-MgO-C1000 catalyst, which can probably be ascribed to the two step reduction of Co_3O_4 (Co_3O_4 to CoO and CoO to Co) with broad particle size distribution.

The ratio of reducible Co to the total Co species in the catalysts was estimated from the TPR profiles by integrating the area under the curves (up to the reduction temperature, e.g., 450 or 750 °C) and normalizing to the total amount of Co available in the catalyst (Table 2). The error in quantifying the total amount of Co in a bulk Co_3O_4 sample by integration of the TPR profile up to 900 °C was less than 10−15%. The amount of reducible Co (as a fraction of the total Co) follows the order of 10Co-MgO-C500-R750 > 10Co-MgO-C500-R450 > 50Co-MgO-C1000-R450 > 10Co-MgO-C1000-R450 as shown in Table 2. These results indicate that higher calcination temperatures result in more stabilization of Co^{2+} and hence a lower extent of Co reduction. In addition, reduction temperature plays an important role with higher reduction temperatures leading to a higher fraction of reduced Co. It should be noted that even after reduction at 750 °C, about 40% of the Co available in the 10Co-MgO-C500-R750 was still present as Co^{2+}.

3.4. XPS. The X-ray photoelectron spectra for the Co-MgO catalysts are shown in Figure 3. Some of the catalysts were reduced ex situ at 750 °C, as indicated next to the XPS spectra, prior to the in situ reduction at 450 °C. The peaks at 778.3 and 780.5 eV are characteristic of Co^0 and Co^{2+} species, respectively.[41,42] It can be seen that lower calcination and higher reduction temperatures led to higher Co^0/Co^{2+} peak ratios, which is in qualitative agreement with the TPR results. The 10% Co-MgO following reduction at 750 °C without any prior calcination (10Co-MgO-NC-R750) showed the most intense Co^0 peak, as shown in Figure 3. The intense Co^{2+} peak for the 10Co-MgO-C500-R750 confirms the presence of significant amount of Co^{2+}, even after reduction at 750 °C. This indicates that upon calcination, even at low temperatures, some of the Co forms CoO-MgO solid solution which becomes difficult to reduce. This is in agreement with the TPR results showing that about 40% Co is nonreducible for 10Co-MgO-C500-R750 (see Table 2). The Co^{2+} incorporated in the MgO lattice is nonreducible and allows us to probe the activity and selectivity of Co^{2+} during ESR.

There are clear differences in the high resolution Co2p core-level spectra for Co^0 metal and Co^{2+} in CoO with respect to the primary peak positions and satellite line shapes. To provide insights into the ratio of Co^0 and Co^{2+} from the Co2p photoemission spectra, the Co^0 and Co^{2+} were fit according to the procedure described in the Experimental Section to quantify the surface Co^0 fraction in the catalysts. Table 2 lists the $Co^0/(Co^0+Co^{2+})$ surface fraction quantified from the XPS spectra in Figure 3. It can be seen that the Co^0 fraction from XPS is in agreement (qualitatively) with that from TPR (Table 2). The difference in absolute numbers between XPS and TPR is likely due to the surface versus bulk nature, respectively, of the two techniques. Therefore, the fraction of Co^0 estimated from XPS will be used in the following sections as it describes more

dx.doi.org/10.1021/cs200014j |ACS Catal. 2011, 1, 279–286

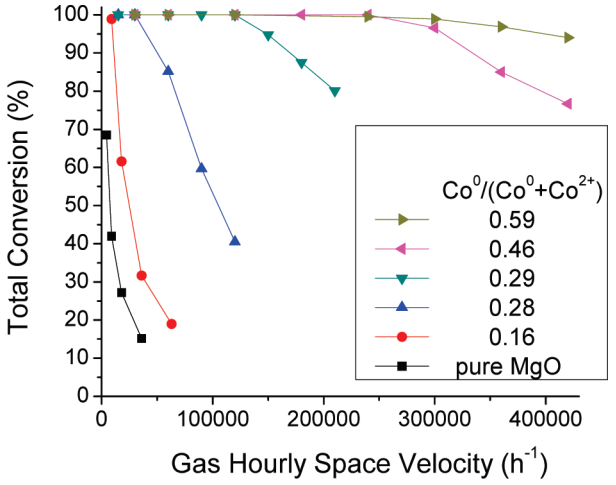

Figure 4. Ethanol conversion as a function of the gas hourly space velocity on different Co-MgO catalysts. Catalysts are labeled according to their surface Co^0 fraction, $Co^0/(Co^0+Co^{2+})$, measured by XPS (see Table 2). Reaction conditions: T = 450 °C, P = 20 psia $H_2O/C_2H_5OH/N_2$ = 10:1:94 molar ($\%_{EtOH}$ = 0.95%).

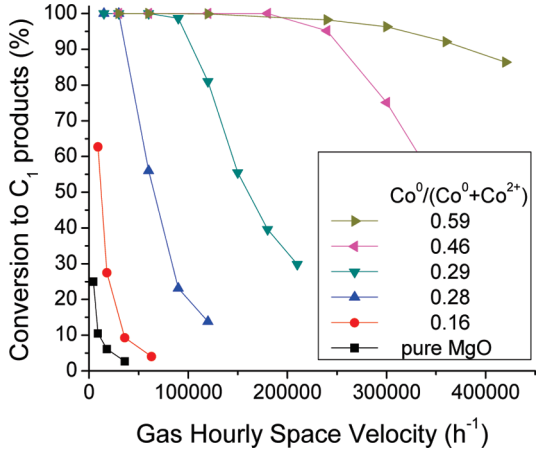

Figure 5. Ethanol conversion to C_1 products (CO_2, CO, CH_4) as a function of the gas hourly space velocity on different Co-MgO catalysts. Catalysts are labeled according to their surface Co^0 fraction, $Co^0/(Co^0+Co^{2+})$, measured by XPS (see Table 2). Reaction conditions: T = 450 °C, P = 20 psia, $H_2O/C_2H_5OH/N_2$ = 10:1:94 molar ($\%_{EtOH}$ = 0.95%).

accurately the difference in Co oxidation state on the surface of catalysts. The Co/Mg atomic ratio is also included in Table 2. For the 10 wt % Co loading, the catalysts calcined at 500 °C exhibited similar Co/Mg ratio (0.29−0.33) while calcination at 1000 °C resulted in higher Co/Mg ratio (0.42). Compared to the lower calcination temperatures, a high calcination temperature resulted in more Co incorporated in the MgO lattice, leading to a higher Co/Mg ratio detected by XPS.

3.5. Catalytic Activity and Selectivity for ESR. The activity for steam reforming of ethanol as a function of gas hourly space velocity (GHSV) over Co-MgO catalysts is shown in Figure 4 and Figure 5 for the total conversion and conversion to C_1 products, respectively. The catalyst activity for the conversion of ethanol correlates with the fraction of Co^0 on the surface as seen in Figure 4. For example, from Figure 4, the GHSV needed to achieve 85% ethanol conversion, is 60,000 and 360,000 h^{-1} for the catalysts having Co^0 fraction of 0.28 and 0.46, respectively. Similarly, from Figure 5, for the catalysts having Co^0 fraction of 0.29 and 0.59, the GHSV required to achieve ~85% conversion to C_1 products was 120,000 and 420,000 h^{-1}, respectively. In other words, to achieve the same conversion, less catalyst amount will be required as the Co^0 fraction increases. These results show that the catalysts with higher Co^0 fraction are more active for ESR, and especially for the C−C bond scission.

Table 3 compares the selectivity to liquid products at a similar total ethanol conversion of 95%. Different space velocities (also listed in Table 3) were used to reach a similar conversion on most catalysts. The addition of Co to MgO reduced the selectivity to liquid products as shown in Table 3. Since all catalysts had some measurable Co^0 with XPS, a lower activity to liquid products could be due to a higher C−C cleavage activity of Co^0 and/or Co^{2+} compared with Mg^{2+}. It can also be seen from Table 3 that the selectivity to liquid products decreases as the fraction of Co^0 present on the surface increases. This is in agreement with the results of conversion to C_1 products, which increases with the Co^0 fraction as shown in Figure 5. These experimental results confirm that Co^0 is more active for C−C bond cleavage than Co^{2+}. On the most active catalyst (10Co-MgO-NC-R750, $Co^0/(Co^0+Co^{2+})$ = 0.59), liquid products (mostly acetaldehyde) appeared only at high space velocity, and the selectivity toward acetaldehyde increased constantly with space velocity, indicating that acetaldehyde is an intermediate during ESR. This is also in agreement with the results reported by Llorca et al.[24]

ESR proceeds via a series of reactions, either dehydrogenation and reforming (eq 1 and/or 6) followed by water gas shift (WGS, eq 5) or dehydrogenation and decomposition (eq 2) followed by methane reforming (reverse reaction in eq 3) and WGS. The desired products from ESR are H_2 and CO_2. CO and CH_4 are undesired products, especially CH_4 since it requires higher temperature for reforming and has a larger effect on H_2 selectivity as seen from eqs 2 through 5 below. Therefore, minimizing ethanol decomposition (eq 2) and CO/CO_2 methanation (eq 3 and 4) along with a high WGS activity are crucial in achieving high selectivities to H_2 and CO_2. Table 4 and 5 compare the selectivities to H_2 and C_1 products at moderate and high ethanol conversions, respectively. Different GHSVs were used to achieve the same conversion to C_1 products on the different catalysts. As discussed above, as the Co^0 fraction in the catalyst increased, higher GHSV was required to achieve the same conversion. The comparison of catalyst selectivity at a similar conversion emphasizes the relative importance of the different reaction pathways, especially since the contribution from the MgO support is negligible. Selectivity to CH_4 was highly dependent on the Co^0 fraction on the surface. An obvious reverse correlation between the selectivity to CH_4 and the $Co^0/(Co^0+Co^{2+})$ surface fraction can be seen. A higher Co^0 fraction on the surface resulted in a lower selectivity to CH_4. These results suggest that methane formation via ethanol decomposition (eq 2) and/or CO/CO_2 methanation (eqs 3 and 4) could be more favored on Co^{2+} than on Co^0. H_2 selectivity is also shown to increase with the Co^0 fraction in the catalyst. From the above results, it can be seen that the catalyst activity and selectivity to H_2 increased with the Co^0 fraction in the catalyst. The highest activity and selectivity to H_2 were achieved on the 10Co-MgO-NC-R750 catalyst which was reduced at a higher temperature without prior calcination. It is possible that elimination of the calcination step weakens the Co

dx.doi.org/10.1021/cs200014j |ACS Catal. 2011, 1, 279–286

Table 3. Liquid Products Selectivity at an Ethanol Conversion of about 95%[a]

			selectivity (%)		
	$Co^0/(Co^0+Co^{2+})$	GHSV (hr^{-1})	acetaldehyde	acetone	total liquids
MgO[b]		4,500	45	14	59
10Co-MgO-C1000-R450	0.16	9,000	3	40	43
50Co-MgO-C1000-R450[c]	0.28	60,000	34	0.7	34.7
10Co-MgO-C500-R450	0.29	150,000	41	0.7	41.7
10Co-MgO-C500-R750	0.46	300,000	22	0.4	22.4
10Co-MgO-NC-R750	0.59	420,000	8	0.1	8.1

[a] Co^0 fraction on the surface, $Co^0/(Co^0+Co^{2+})$, was quantified by XPS. Reaction conditions: T = 450 °C, P = 20 psia $H_2O/C_2H_5OH/N_2$ = 10:1:94 molar ($\%_{EtOH}$ = 0.95%). [b] conversion =70% [c] conversion =85%

Table 4. Selectivity to C_1 Products at Ethanol Conversion (to C_1) between 50−60%[a]

			selectivity to C_1 products (%)		
	$Co^0/(Co^0+Co^{2+})$	GHSV (hr^{-1})	CH_4	CO	CO_2
MgO[b]		4,500	16.3	49.7	33.9
10Co-MgO-C1000-R450	0.16	9,000	19.7	31.7	48.6
50Co-MgO-C1000-R450	0.28	60,000	17.6	40.9	41.5
10Co-MgO-C500-R450	0.29	150,000	11	54.5	34.5
10Co-MgO-C500-R750	0.46	360,000	8.3	47.7	44
10Co-MgO-NC-R750	0.59	NA	NA	NA	NA

[a] NA: not available, 50% conversion was not achieved on this catalyst because of its high activity. Co^0 surface fraction, $Co^0/(Co^0+Co^{2+})$ was quantified by XPS. Reaction conditions: T = 450 °C, P = 20 psia, $H_2O/C_2H_5OH/N_2$ = 10:1:94 molar ($\%_{EtOH}$ = 0.95%). [b] Conversion = 25%.

Table 5. Selectivity to C_1 Products and H_2 at Ethanol Conversion (to C_1) of ∼95%[a]

			selectivity to C_1 products (%)			
	$Co^0/(Co^0+Co^{2+})$	GHSV (hr^{-1})	CH_4	CO	CO_2	H_2 selectivity (%) [b]
MgO		NA	NA	NA	NA	NA
10Co-MgO-C1000-R450	0.16	NA	NA	NA	NA	NA
50Co-MgO-C1000-R450	0.28	15,000	16	22.1	61.9	81
10Co-MgO-C500-R450	0.29	90,000	13.1	48.9	38	76
10Co-MgO-C500-R750	0.46	240,000	10.1	31.9	58	85
10Co-MgO-NC-R750	0.59	300,000	9.2	15.1	75.7	93

[a] NA: not available, 95% conversion could not be achieved on these catalysts because of their low activity. Co^0 surface fraction, $Co^0/(Co^0+Co^{2+})$ quantified by XPS. Reaction conditions: T = 450 °C, P = 20 psia, $H_2O/C_2H_5OH/N_2$ = 10:1:94 molar ($\%_{EtOH}$ = 0.95%). [b] Defined as (mole H_2/mol ethanol reacted)/6.

interaction with MgO, which consequently results in a higher Co^0 fraction after the catalyst reduction.

$$C_2H_5OH + 3H_2O \rightarrow 2CO_2 + 6H_2 \quad (1)$$

$$C_2H_5OH \rightarrow CO + CH_4 + H_2 \quad (2)$$

$$CO + 3H_2 \leftrightarrow CH_4 + H_2O \quad (3)$$

$$CO_2 + 4H_2 \leftrightarrow CH_4 + 2H_2O \quad (4)$$

$$CO + H_2O \leftrightarrow CO_2 + H_2 \quad (5)$$

$$C_2H_5OH + 2H_2O \rightarrow CO_2 + CO + 5H_2 \quad (6)$$

To provide insight into the reaction pathways for ESR on Co^0 and Co^{2+}, catalyst selectivities to CH_4, CO, and CO_2 as a function of GHSV are compared for two catalysts with low and high surface Co^0 fractions (Figure 6). On the catalyst with a lower Co^0 fraction (Figure 6a), selectivities to CH_4 and CO increase while the selectivity to CO_2 decreases as the GHSV increases. Additionally, selectivities to CO and CH_4 are higher than the equilibrium values of 7.3% and 10.4%, respectively. These results indicate that on the catalysts with more Co^{2+} surface sites, CH_4 and CO are the primary products, likely because of ethanol decomposition (eq 2). The fact that CH_4 selectivity is not close to 50% may suggest either CH_4 reforming and/or reforming of ethanol (eq 6) are occurring.

On the catalyst with a higher Co^0 fraction (Figure 6b), the trend for CO and CO_2 selectivities was found to be similar to that on the catalyst with a lower Co^0 fraction. However, CH_4

dx.doi.org/10.1021/cs200014j |ACS Catal. 2011, 1, 279–286

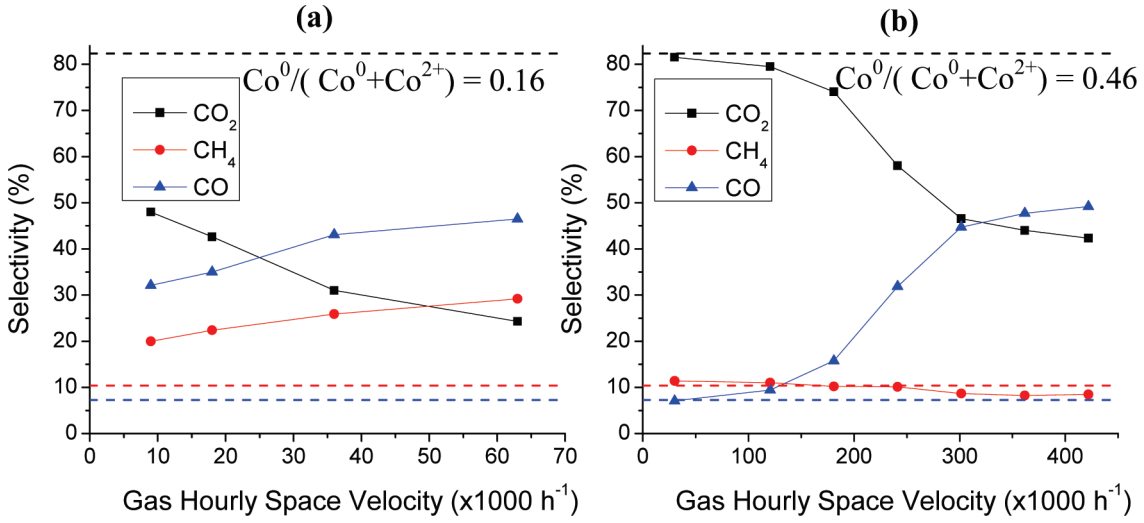

Figure 6. Selectivity to C_1 products (CO_2, CO, CH_4) as a function of the gas hourly space velocity on 10Co-MgO-C1000-R450 (left) and 10Co-MgO-C500-R750 (right). The catalysts are labeled according to their surface Co^0 fraction, $Co^0/(Co^0+Co^{2+})$, measured by XPS (see Table 2). Reaction conditions: T = 450 °C, P = 20 psia, $H_2O/C_2H_5OH/N_2$ = 10:1:94 molar ($\%_{EtOH}$ = 0.95%). Dashed lines represent the thermodynamic equilibrium selectivity.

Table 6. Effect of H_2 Amount in the Feed on the Selectivity of 10Co-MgO-NC-R750 ($Co^0/(Co^0+Co^{2+})$ = 0.59) during WGS[a]

H_2% in the inlet	CO conversion (%)	CO_2 selectivity (%)	CH_4 selectivity (%)
10	77	99.5	0.5
44	53	97	3

[a] Reaction conditions: P = 18 psia, T = 450 °C, H_2O = 33%, CO% = 13%, H_2 = 10 or 44%, balance N_2, GHSV = 124,000 h^{-1}.

selectivity slightly decreases (from 11% to 8.5%) with increasing GHSV and remains close to (but below) the equilibrium value. Because of the weak dependence of CH_4 selectivity on the space velocity, it is not possible to determine whether CH_4 was formed by ethanol decomposition or methanation of CO on the catalyst with more Co^0 sites, especially since the selectivity was close to the equilibrium value.

To provide an understanding of the reaction pathway for methane formation, in particular to probe whether methanation of CO (eq 3) is responsible for CH_4 formation on catalysts with high Co^0 surface fraction, we conducted WGS tests with two different concentrations of H_2 in the feed. Table 6 summarizes CO conversion and selectivities to CO_2 and CH_4 with 10 and 44% H_2 in the reactants. Methane selectivity increased with the H_2 concentration in the inlet; however, it was still very low (3%) even with 44% H_2 in the feed, and the catalyst was very selective toward WGS. These results suggest that although CO (or CO_2) methanation reaction is much slower compared to WGS under the reaction conditions studied, its contribution to methane formation on the catalysts with high Co^0 fractions cannot be excluded. From these results and the results in Figure 6b, we can conclude that steam reforming of ethanol to CO and CO_2 (eq 6) followed by WGS is the major pathway on catalysts with high Co^0 fraction during ESR.

A similar experiment was performed on the 10% Co/MgO catalyst calcined at 1000 °C which has a low Co^0 fraction as discussed above. However, the activity for WGS and CO methanation

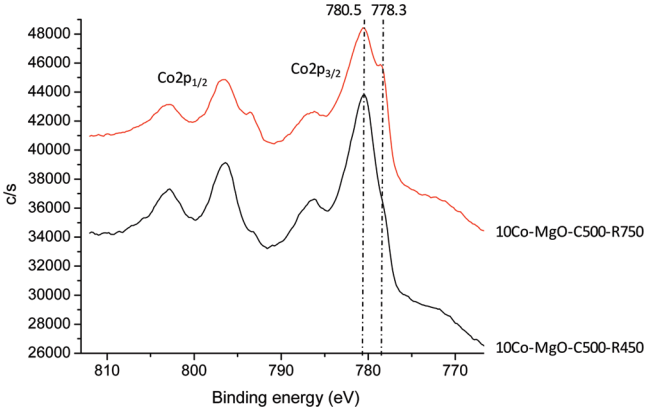

Figure 7. X-ray spectra recorded in the Co 2p region for the Co-MgO catalysts after exposure to a mixture of $H_2/H_2O/N_2$ with a molar ratio 1:1:49. All catalysts were reduced in situ at 450 °C for 1 h prior to the exposure to the $H_2/H_2O/N_2$ mixture. Peaks at 778.3 and 780.5 eV, respectively, are characteristic of Co^0 and Co^{2+}.

in the presence of H_2 (at the lowest possible GHSV) was very low, and therefore further confirming that ethanol composition pathway (eq 2) is dominating on the catalysts with high Co^{2+} fraction.

It is worth noting that oxidation of Co by H_2O was found to be facile through the following reaction, $H_2O + Co^0 \rightarrow H_2 + CoO$. This was evident when H_2 was detected following the introduction of steam on the 10Co/MgO-C500-R750 catalyst (data not shown). Figure 7 shows the XPS spectra collected for two catalysts, namely, 10Co/MgO-C500-R450 and 10Co/MgO-C500-R750 after exposure to a H_2/H_2O mixture. The exposure to H_2/H_2O resulted in the partial oxidation of Co in both catalysts. However, the trend in $Co^0/(Co^0+Co^{2+})$ remains the same as that after reduction, with the $Co^0/(Co^0+Co^{2+})$ being higher for the Co/MgO-C500-R750 compared to the Co/MgO-C500-R450 catalyst. Therefore, even though oxidation by H_2O lowers the fraction of Co^0, the main conclusion that Co^0 is much more active and selective than Co^{2+} in ESR remains the

dx.doi.org/10.1021/cs200014j |ACS Catal. 2011, 1, 279–286

same, whether Co^{2+} is nonreducible (in the MgO lattice) or reducible (produced on the Co particle from oxidation by H_2O). The oxidation of Co^0 by H_2O under ESR reaction conditions could be responsible for the CH_4 produced because of the increase in Co^{2+} sites. Therefore, stabilizing Co^0 against oxidation by steam under reaction conditions is crucial in achieving high activity and selectivity to H_2. The use of promoters to stabilize Co against oxidation by H_2O is currently being studied and will be the subject of a subsequent publication.

4. CONCLUSIONS

The roles of Co^0 and Co^{2+} in ESR pathways were investigated on Co/MgO catalysts. The Co^0 fraction was varied using different calcinations and reduction treatments. The bulk and surface Co^0 fraction were quantified by TPR and in situ XPS. It was found that Co^0 is much more active than Co^{2+} for ethanol conversion, C−C cleavage, and the WGS reactions. The reaction pathways during ESR are shown to be different on Co^0 and Co^{2+}. Ethanol reforming to CO and CO_2 followed by WGS appears to be the dominant pathway on Co^0, while ethanol decomposition to methane seems to be dominant on Co^{2+}. Minimization of Co^{2+} and stabilization of Co^0 against oxidation are crucial to achieve high H_2 productivity and yield.

AUTHOR INFORMATION

Corresponding Author

*E-mail: yong.wang@pnl.gov. Phone: +1-509- 371-6273.

ACKNOWLEDGMENT

The authors would like to thank the financial support from U. S. Department of Energy (Grant DE-FG02-05ER15712). A portion of the research was performed using EMSL, a national scientific user facility sponsored by the Department of Energy's Office of Biological and Environmental Research located at Pacific Northwest National Laboratory.

REFERENCES

(1) Llorca, J.; Homs, N.; Sales, J.; de la Piscina, P. R. *J. Catal.* **2002**, *209*, 306–317.
(2) Fatsikostas, A. N.; Kondarides, D. I.; Verykios, X. E. *Catal. Today* **2002**, *75*, 145–155.
(3) Breen, J. P.; Burch, R.; Coleman, H. M. *Appl. Catal., B* **2002**, *39*, 65–74.
(4) Liguras, D. K.; Kondarides, D. I.; Verykios, X. E. *Appl. Catal., B* **2003**, *43*, 345–354.
(5) Montini, T.; De Rogatis, L.; Gombac, V.; Fornasiero, P.; Graziani, M. *Appl. Catal., B* **2007**, *71*, 125–134.
(6) Jacobs, G.; Keogh, R. A.; Davis, B. H. *J. Catal.* **2007**, *245*, 326–337.
(7) Goula, M. A.; Kontou, S. K.; Tsiakaras, P. E. *Appl. Catal., B* **2004**, *49*, 135–144.
(8) Bi, J. L.; Hong, Y. Y.; Lee, C. C.; Yeh, C. T.; Wang, C. B. *Catal. Today* **2007**, *129*, 322–329.
(9) Guarido, C. E. M.; Cesar, D. V.; Souza, M.; Schmal, M. *Catal. Today* **2009**, *142*, 252–257.
(10) Homs, N.; Llorca, J.; de la Piscina, P. R. *Catal. Today* **2006**, *116*, 361–366.
(11) Denis, A.; Grzegorczyk, W.; Gac, W.; Machocki, A. *Catal. Today* **2008**, *137*, 453–459.
(12) Wang, F.; Li, Y.; Cai, W. J.; Zhan, E. S.; Mu, X. L.; Shen, W. J. *Catal. Today* **2009**, *146*, 31–36.
(13) Fajardo, H. V.; Probst, L. F. D.; Carreno, N. L. V.; Garcia, I. T. S.; Valentini, A. *Catal. Lett.* **2007**, *119*, 228–236.
(14) Fatsikostas, A. N.; Verykios, X. E. *J. Catal.* **2004**, *225*, 439–452.
(15) Frusteri, F.; Freni, S.; Chiodo, V.; Spadaro, L.; Bonura, G.; Cavallaro, S. *J. Power Sources* **2004**, *132*, 139–144.
(16) Frusteri, F.; Freni, S.; Chiodo, V.; Spadaro, L.; Di Blasi, O.; Bonura, G.; Cavallaro, S. *Appl. Catal., A* **2004**, *270*, 1–7.
(17) Llorca, J.; de la Piscina, P. R.; Dalmon, J. A.; Sales, J.; Homs, N. *Appl. Catal., B* **2003**, *43*, 355–369.
(18) Song, H.; Ozkan, U. S. *J. Catal.* **2009**, *261*, 66–74.
(19) Wang, H.; Ye, J. L.; Liu, Y.; Li, Y. D.; Qin, Y. N. *Catal. Today* **2007**, *129*, 305–312.
(20) Wang, C. B.; Lee, C. C.; Bi, J. L.; Siang, J. Y.; Liu, J. Y.; Yeh, C. T. *Catal. Today* **2009**, *146*, 76–81.
(21) Lin, S. S. Y.; Kim, D. H.; Ha, S. Y. *Appl. Catal., A* **2009**, *355*, 69–77.
(22) Llorca, J.; Dalmon, J. A.; de la Piscina, P. R.; Homs, N. *Appl. Catal., A* **2003**, *243*, 261–269.
(23) Batista, M. S.; Santos, R. K. S.; Assaf, E. M.; Assaf, J. M.; Ticianelli, E. A. *J. Power Sources* **2003**, *124*, 99–103.
(24) Llorca, J.; Homs, N.; de la Piscina, P. R. *J. Catal.* **2004**, *227*, 556–560.
(25) O'Shea, V. A. D.; Homs, N.; Pereira, E. B.; Nafria, R.; de la Piscina, P. R. *Catal. Today* **2007**, *126*, 148–152.
(26) Tuti, S.; Pepe, F. *Catal. Lett.* **2008**, *122*, 196–203.
(27) Cavallaro, S.; Mondello, N.; Freni, S. *J. Power Sources* **2001**, *102*, 198–204.
(28) Cimino, A. *Mater. Chem. Phys.* **1985**, *13*, 221–241.
(29) Chambers, S. A.; Farrow, R. F. C.; Maat, S.; Toney, M. F.; Folks, L.; Catalano, J. G.; Trainor, T. P.; Brown, G. E. *J. Magn. Magn. Mater.* **2002**, *246*, 124–139.
(30) Shirley, D. A. *Phys. Rev. B* **1972**, *5*, 4709-&.
(31) Moulder, J. F.; Stickle, W. F.; Sobol, P. E.; Bomben, K. *Handbook of X-ray Photoelectron Spectroscopy*, 2nd ed.; Perkin-Elmer, Physical Electronics Division: Eden Prairie, MN, 1992.
(32) Dupin, J. C.; Gonbeau, D.; Benqlilou-Moudden, H.; Vinatier, P.; Levasseur, A. *Thin Solid Films* **2001**, *384*, 23–32.
(33) Foelske, A.; Strehblow, H.-H. *Surf. Interface Anal.* **2000**, *29*, 548–555.
(34) Karim, A. M.; Su, Y.; Sun, J.; Yang, C.; Strohm, J. J.; King, D. L.; Wang, Y. *Appl. Catal., B* **2010**, *96*, 441–448.
(35) Cimino, A.; Deangelis, B. A.; Minelli, G. *Surf. Interface Anal.* **1983**, *5*, 150–154.
(36) Belambe, A. R.; Oukaci, R.; Goodwin, J. G. *J. Catal.* **1997**, *166*, 8–15.
(37) Wang, H. Y.; Ruckenstein, E. *Appl. Catal., A* **2001**, *209*, 207–215.
(38) Batista, M. S.; Santos, R. K. S.; Assaf, E. M.; Assaf, J. M.; Ticianelli, E. A. *J. Power Sources* **2004**, *134*, 27–32.
(39) Jongsomjit, B.; Panpranot, J.; Goodwin, J. G. *J. Catal.* **2001**, *204*, 98–109.
(40) Khodakov, A. Y.; Lynch, J.; Bazin, D.; Rebours, B.; Zanier, N.; Moisson, B.; Chaumette, P. *J. Catal.* **1997**, *168*, 16–25.
(41) Riva, R.; Miessner, H.; Vitali, R.; Del Piero, G. *Appl. Catal., A* **2000**, *196*, 111–123.
(42) Khassin, A. A.; Yurieva, T. M.; Kaichev, V. V.; Bukhtiyarov, V. I.; Budneva, A. A.; Paukshtis, E. A.; Parmon, V. N. *J. Mol. Catal A: Chem.* **2001**, *175*, 189–204.